IJTBI
International Journal of Technovation and Business Insights
Volume 01, Issue 02, October -December 2025
ISSN: 3107-7900, P.CODE: 25/1-2/04
DOI: https://doi.org/10.5281/zenodo.22305163

NONLINEAR ANOMALOUS HALL EFFECT FOR NE´EL VECTOR DETECTION

PARLAPALLI PRABHAKAR, *Associate Professor & HOD, Dept of ECE*,
TRINITY COLLEGE OF ENGINEERING & TECHNOLOGY, PEDDAPALLI

ABSTRACT : Ne'el vectors serve as state variables in cutting-edge antiferromagnetic (AFM) spintronic devices. Antidamping spin-orbit torques (SOTs) have been demonstrated to influence the Ne'el vectors of antiferromagnets exhibiting specific symmetries. The precise whereabouts of the Ne'el vector are still undisclosed. The Ne'el vector in balanced antiferromagnets with antidamping spin-orbit torque (SOT) can be determined using the nonlinear anomalous Hall effect. The nonlinear anomalous Hall effect arises from the substantial dipole of Berry curvature resulting from the interplay between spin-orbit interaction and magnetic crystal group symmetry in antiferromagnetic materials. Examine the CuMnSb half-Heusler alloy. This alloy's antidamping spin-orbit torque (SOT) modifies the Ne'el vector. The nonlinear anomalous Hall effect (AHE) in CuMnSb can produce a Hall voltage in a conventional laboratory setting. This is corroborated by density-functional theory. The orientation of the Ne'el vector is closely linked to the dipole of the Berry curvature. A unique method for calculating the Ne'el vector utilizing the nonlinear anomalous Hall effect (AHE) is devised. We expand the scope of materials that may be examined using AFM spintronics and suggest novel methodologies for assessing intricate Berry curve phenomena.

Keywords: *Anomalous Hall Effect, Magnetic Materials, Neel Order*

1. INTRODUCTION

For solid-state systems, spintronics involves manipulating and recognizing spin characteristics. Multilayer ferromagnetic structures, which are essential to spintronics, have lately revealed new behavior in various configurations. Recent industry initiatives have focused on power consumption and device shifting efficiency. Antiferro magnets in spintronic applications are better than ferromagnets due to their mobility, lack of stray fields, and inability to rapidly change magnetic fields [2-6]. A new study indicates that field-like spin-orbit torques (SOTs) can modify the Ne'el vector in P T symmetric antiferromagnets. T and P represent time reversal and spatial inversion symmetry, respectively. These compounds include MnPd2, CuMnAs, and Mn2Au. Optical methods determine the direction of the Ne'el vector. The particular needs of these additional possibilities can make gadget use difficult. A working AFM spintronic system requires speedy Ne'el vector determination utilizing electricity and ordinary laboratory equipment. A material's electrical band structure's berry curve is unchanging.It controls the anomalous Hall effect (AHE) appearance [18,19]. The anomalous Hall effect (AHE), which impacts the entire Brillouin zone, can be non-zero in materials when the time reversal symmetry T is violated [20]. Because the wave vector k and the process

Volume 01, Issue 02, October -December 2025
ISSN: 3107-7900, P.CODE: 25/1-2/04
DOI: https://doi.org/10.5281/zenodo.22305163

T k k are not symmetrical under T. The weird Hall effect (AHE) in antiferromagnets is caused by T symmetry disruption. A Ne'el vector can be calculated. Figure 1(a) shows the uncommon Hall effect (AHE) of Mn X and other noncollinear antiferromagnets.

In asymmetric antiferromagnets like CuMnSb, the antidamping spin-orbit torque (SOT) can occasionally modify the Ne'el vector [8, 10, 13, 1]. Antiferromagnets' lack of net magnetization and fast magnetization variation make them difficult to identify for the Ne'el vector with ordinary magnetometers and magnetic resonance. This study uses anisotropic magnetoresistance (AMR) to calculate Ne'el vector flips.This effect slows data reading, but it's minimal.Optical methods precisely determine the N'eel vector direction.The particular needs of these additional possibilities can make gadget use difficult. Using conventional laboratory equipment to build an AFM spintronic system and efficiently determine the N'eel vector is perfect. A material's electrical band structure's berry curve is unchanging.It controls the anomalous Hall effect's visibility. The Brillouin zone total may not be zero if a material's time reversal symmetry T is broken. This is the odd Hall effect. Because of its odd symmetry under the transformation T, T k = k, where k is the wave vector. Due to their lack of T symmetry, antiferromagnets do not experience the nonvanishing AHE. N'eel vectors are found this way. AHEs were recently reported in collinear antiferromagnets like Mn3X (X = Ga, Ge, Sn, or Ir) and Mn3AN (A = Ga, Zn, Ag, or Ni) with a certain crystal lattice arrangement of nonmagnetic atoms. Due to the small local moment misalignment, these combinations show the net magnetization M. One major issue is that no magnetic group symmetry operation (T O, where O is a crystal space group symmetry operation) can make M equal to zero, as proven by T O M 14 M.

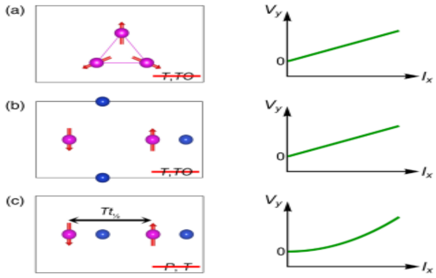

FIG. 1. In equilibrium magnetic fields, antiferromagnetic materials display the linear anomalous Hall effect (AHE).

A unique nonlinear anomalous Hall effect can overcome this problem. In magnetic systems with time-reversal symmetry breakdown, the linear anomalous Hall effect (AHE) shows a direct relation between Hall voltage and applied electric field. Unlike this occurrence, the nonlinear anomalous Hall effect (AHE) shows that the applied electric field affects the Hall voltage second-order. Certain nonmagnetic materials undergo symmetrical changes over time. CuMnSb crystal structure, belonging to F4¯ 3m space group, displays nonlinear anomalous Hall effect (AHE). Below 55 K, materials have type-II collinear antiferromagnetic (AFM) order. Mn atoms in the plane have homogeneous magnetic moments. As shown in Figure 2(a), adjacent planes have different orientations. Axis and Ne'el vector are orthogonal. The antiferromagnetic (AFM) ordering reduces symmetry, creating the magnetic space group RI3c.According to Figure 2(b), the CuMnSb compound has rhombohedral primitive cells with axis

Volume 01, Issue 02, October -December 2025
ISSN: 3107-7900, P.CODE: 25/1-2/04
DOI: https://doi.org/10.5281/zenodo.22305163

symmetry.

The P∫ symmetry is impaired by three mirror reflections: g∫1¯10, gɆ1¯01, and the Berry direction. Curvature dipole D causes electric current-carrying systems to move at unusual speeds. In respect to the nonlinear anomalous Hall effect, researchers have largely studied nonmagnetic materials that keep their T-symmetry. The thought of using it to AFM materials lacking T^ symmetry is intriguing and helpful. This would enable AFM spintronics-critical property observations across a wider range. Spin-orbit torque (SOT) antidamping can control the N'eel vector, and most corrected antiferromagnets should have a nonlinear anomalous Hall effect. These are the letter's main issues. First-principles density-functional-theory (DFT) simulations showed that the CuMnSb half-Heusler alloy has a large nonlinear anomalous Hall effect (AHE) from a restricted Berry curvature dipole. The phenomena is observed when a polar axis and T^^t1=2 symmetry are present. The equation 1=2 shows half the unit cell displacement. The orientation of the antiferromagnetic (AFM) N'eel vector determines the correlation between the Berry curve dipole and the non-linear anomalous Hall effect (AHE). Using this correlation, one can determine the N'eel vector in similar compounds. How is the density of the Berry curvature dipole tensor d determined? Using the formula dbd = - (∂f0/∂kb)d, where kb is the Cartesian component of the wave vector and Ωd is the Berry curvature component. Fermi distribution stable state is f0. A nonlinear anomalous Hall effect (AHE) occurs in antiferromagnets with a less symmetrical center due to Pᶬ. In non-magnetic systems, gyrotropic symmetry standards are essential [36, 55, 56]. The results show that most compensated antiferromagnets with anti-damping spin-orbit torque (SOT) meet the nonlinear anomalous Hall effect (AHE) symmetry requirements. The Bilbao MagnData found that 118 of the 123 noncenterrosymmetric compensated antiferromagnets have magnetic space groups with measurable Berry curvature dipoles. References 57 and 58 confirm this. In Figure 1(c), the nonlinear anomalous Hall effect (AHE) is observed in an antiferromagnet with T]t1=2 symmetry and a polar axis. This is reasonable as T^t1=2 is applied without changing d, resulting in T^t1=2dðkÐ ⊲ dǚ−kÐ. The CuMnSb half-Heusler metal may aid spin-orbit torque. It is an antiferromagnetic metal. Figures 2(a) and 2(b) show CuMnSb arrangement. The crystal is part of the F43¯ m space group with Miller indices. Type-II collinear antiferromagnetic (AFM) order exists below 55 K. Due to their structure, Mn atoms have parallel magnetic moments within the plane, whereas antiparallel magnetic moments between planes are shown in Figure 2(a). In this case, the crystal lattice's direction orientation conflicts with the N'eel vector. AFM order completion causes symmetry reduction, forming the RI3c magnetic space group. Three glide mirror reflections of the CuMnSb rhombohedral primitive cell are shown in Figure 2(b). Values are gˆ110¯, gɆ101¯, and g.011¯. Additionally, it has a triple rotation around the axis (Č3). To obtain these reflections, we use a half-unit cell translation (ˆt1=2) and a mirror symmetry matrix (Mˆ l). At temperatures below 34 K, the N'eel vector aligns with the direction at μ 11° [14,60]. The

IJTBI
International Journal of Technovation and Business Insights
Volume 01, Issue 02, October -December 2025
ISSN: 3107-7900, P.CODE: 25/1-2/04
DOI: https://doi.org/10.5281/zenodo.22305163

deviation affects Cˆ 3, gE101 ¯, and gE011 ¯ symmetries. The remaining option, gE110 ¯, creates the magnetic space group Ccc.

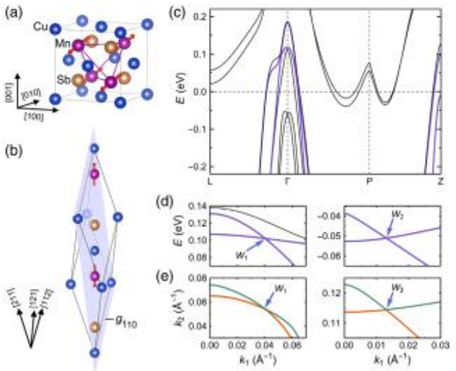

FIG. 2. (AFM analysis of CuMnSb's magnetic structure shows a rhombohedral basic cell (b) and a cube-shaped unit cell (a). Red lines show where Mn's magnetic moments are. An aircraft with a light blue paint job represents the glide plane g∫110 ¯. The spectrum shows CuMnSb waves near the EF on the left. The wave shapes are visible on the right side of the graph at Weyl points W1 (k2 = 0.054 and k3 = 0.004(-1)). Two of the cube grid's three dots are separated. The coordinates of these locations are [110 ¡], [1¡ 1 2¡], and the purple lines in (c) and (d) depict the two Weyl point bands. A narrow line could represent Fermi energy on paper. Fermi surfaces are evident at -0.051 eV on the right and 0.004 and 0.081 Å−1 on the left. Two surfaces intersect at Weyl points.

Rounds later used the number. Considering T•ˆt1=2, both CuMnSb's AFM phases are positively polarized and symmetrical. The heated antiferromagnetic (AFM) phase of CuMnSb is examined first. Reference states that Mn's magnetic moment should be 3.93 ± 0.1 µB, which matches the actual value of 3.9 ± 0.1 µB. The lattice constant is a = 6.075 Å, as explained. Figure 2(c) shows expected band structure. Six bands travel through the Fermi energy EF. The 3d electrons released by Mn are the main cause (Fig. S1). High dispersion is observed at the ¾ point and in the other three outer bands. When moving in the ¾-Z direction, four pockets-like holes will form. At the conduction band's base, the interband gap is barely noticeable. Thus, electron pockets appear halfway between the Brillouin zone's two sections (Fig. S1). Band structure crosses and anticrosses at Fermi energy. Purple lines indicate the second and third valence band crossings in Figures 2(c) and 2(d). Figure 2(d) shows two Weyl points. At E = 0.102 eV (W1) and E = -0.051 eV (W2), respectively. Band crossings tilt at Weyl points. Figure 2(e) indicates that W1 and W2 are where the Fermi pockets intersect. These computations determine type II Weyl fermions (W1 and W2). Six sets of W1 and W2 Weyl fermions are depicted in the center of the Brillouin zone in Figure S1. To produce these sets, change W1 and W2 for T³ˆt1=2, C† 3, and glide symmetry.

A non-linear Hall reaction will be explored next. Gravity pulls charged objects to electric fields.

$$E_c = \mathrm{Re}\{\mathcal{E}e^{i\omega t}\}$$

when the energy E and frequency ó vary, alters the current in a non-linear manner.

$$J_a = \mathrm{Re}\{J_a^{(0)} + J_a^{(2)}e^{i2\omega t}\},$$

where

$$J_a^{(0)} = \chi_{abc}^{(0)}\mathcal{E}_b\mathcal{E}_c^*$$

give details regarding the variation of the current.

$$J_a^{(2)} = \chi_{abc}^{(2)}\mathcal{E}_b\mathcal{E}_c^*$$

the starting point of the second harmonic motion. The symmetrical system's reaction factors are linearly proportional to time, with a value of 36.

Volume 01, Issue 02, October -December 2025
ISSN: 3107-7900, P.CODE: 25/1-2/04
DOI: https://doi.org/10.5281/zenodo.22305163

$$\chi^{(0)}_{abc} = \chi^{(2)}_{abc} = -\epsilon_{adc}\frac{e^3\tau D_{bd}}{2\hbar^2(1+i\omega\tau)}, \qquad (1)$$

$$\chi^{(0)}_{abc} = \chi^{(2)}_{abc} = -\epsilon_{adc}\frac{e^3\tau D_{bd}}{2\hbar^2(1+i\omega\tau)}, \qquad (1)$$

where τ is the relaxation time, and D_{bd} is the Berry curvature dipole defined as

$$D_{bd} = \int \frac{d^3k}{(2\pi)^3} d_{bd} = -\int \frac{d^3k}{(2\pi)^3} \sum_n \frac{\partial E_{nk}}{\partial k_b} \Omega^d_{nk} \frac{\partial f_0}{\partial E_{nk}}. \qquad (2)$$

Here, Enk stands for the energy of the k-point and the nth band. The Berry curve for the nth band is described in [20,22].

$$\Omega^d_{nk} = i\epsilon_{abd} \sum_{m\neq n} \frac{\langle n|\frac{\partial H}{\partial k_a}|m\rangle\langle m|\frac{\partial H}{\partial k_b}|n\rangle}{(E_{nk}-E_{mk})^2}. \qquad (3)$$

There are strange behaviors for the number ©d nk when Tˆ symmetry is present, but normal behaviors when Pˆ symmetry is present. But when you look at both the Pˆ and Tˆ symmetries, the part ∂Enk=∂kb acts in a strange way .This means that the term "dbd" in Equation (2) acts the way it should in a system that isn't magnetic and is flat around a center point in terms of Tˆ. It is possible to see the nonlinear anomalous Hall effect (AHE) when Dbd is not zero. CuMnSb is an antiferromagnetic material that has a half-time translation symmetry that stays the same (T†ˆt1=2). It's this symmetry that changes the volume derivative of the wave vector (∂Ωd nk) and the energy derivative (∂Enk=∂kb). Also, the fact that there is a polar axis ensures that D will not be zero. Because of this, a low Dbd is likely to happen in this kind of antiferromagnet. Table SII in the Supplemental Material [43] shows that the D tensor in the AFM phase without canting only has one independent element. In order to be sure of our results, we look at Dxz, which is directly related to Jy ¼ φyxxE2 x. If you look at an electric field in the x direction, it makes a transversal nonlinear Hall current, Dxz. Following the [010] direction, the current in question goes down the y-axis. Figure 3(a) and 3(b) show how Dxz is projected onto the k1-k2 plane. It can be found by integrating R ŏdk3=2π^dxz at E = 0.102 eV (Fig. 3(a)) and E = 0.051 eV (Fig. 3(b)). The only thing that affects Dxz is the Fermi pockets, as shown by Equation (2), which makes Dxz a feature of the Fermi surface. It is clear that the Fermi pockets in the conduction bands don't make a difference when compared to the valence bands. This impact happens because electrons are scattering more strongly at the upper boundary of the valence bands, which makes the speeds go up.

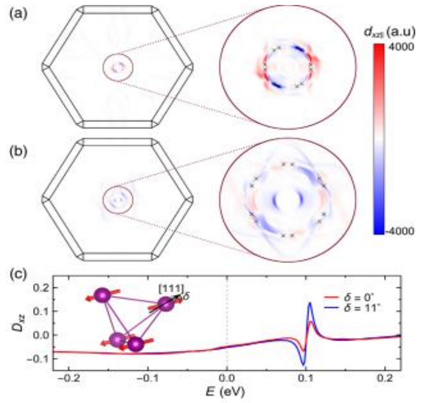

FIG. 3. (a),(b) The projections of the Berry curvature dipole on k_1-k_2 plane at (a) $E = 0.102$ and (b) $E = -0.051$ eV. Black cross symbols denote position of the Weyl fermions. (c) The D_{xz} as a function of energy for the AFM phase without (red line) and with (blue line) canting of the Néel vector. (Inset) Schematic showing the canting.

The equation vx = Enk = kx is seen in Figure 2(c). The minimal changes in valence band at the Fermi level (EF) result in a higher value for z nk, as indicated in Equation. The graph in Figure 3(c) illustrates that there is an inverse relationship between Dxz and energy, meaning that as energy declines, Dxz increases. The enlargement of the central Fermi surfaces arises due to the presence of the valence bands. According to our data, at EF, the value of Dxz was around -0.048. The value of this figure, however, can be reduced to -0.080 with appropriate

Volume 01, Issue 02, October -December 2025
ISSN: 3107-7900, P.CODE: 25/1-2/04
DOI: https://doi.org/10.5281/zenodo.22305163

treatment [Fig. 3(c)]. Based on statistical research, these metals exhibit no discernible distinction from non-magnetic metals [38, 39]. It is important to consider that the two separate Weyl fermions, W1 and W2, have discrete contributions to Dxz. The regulation of Dxz is greatly influenced by the states surrounding W1 at an energy level of E = 0.102 eV, as depicted in Figure 3(a) and Supplemental Material Fig. S.Figure 3(c) illustrates that this event results in an anomalous shape of the Dxz curve at this particular energy. The slight curvature of the Weyl cones creates the perception that W2 has a negligible impact, as depicted in Figure 3(b)[43]. What is the cause of this occurrence? The abnormality in the Dxz curve at E 0.051 eV is hidden in [Fig. 3(c)]. Although EF is close to W1 and W2, they are not connected to Dxz since D is a characteristic of the Fermi surface. The peculiar D shape of EF is a consequence of its dispersive band structure, favorable symmetry, and robust spin-orbit interaction. This object exhibits an 11° angular deviation towards the direction when maintained at room temperature. Figure S2 demonstrates that the band pattern undergoes negligible alteration as a result of this slight tilt.

Fig. S2 shows that the number and position of Weyl fermions are changed due to the violation of the gˆ101¯, gȄ011¯, and Cˆ 3 symmetries. Figure 3(c) and Supplementary Material Figure S2 [43] show that the energy dependence of Dxz in this antiferromagnetic (AFM) phase is almost same to that in the phase without canting, with the exception of a few more prominent peaks above the Fermi energy (EF) caused by the modified arrangement of the Weyl points. The symmetry break affects the D tensor and changes the amplitude of Dxy and Dxz (Supplemental Material Table SII [43]). With more pronounced canting, the margin might grow substantially. Take the half-Heusler metal GdMnBi as an example; when the canting angle is ½ • 90°, the value of Dxy is 0.072, which is much greater than Dxz (Table SII [43]). Since Dxy and Vz are known to be correlated, non-linear Hall responses on the y and z axes result from a large disparity between the two variables. Using this method, one can find the N'eel vector's canting. Because it depends on the N'eel vector's orientation, the nonlinear anomalous Hall effect (AHE) can be used to find the Berry curvature dipole. The CuMnSb compound displays type-II antiferromagnetic (AFM) ordering, which has an energy structure comparable to that seen when the N'eel vector is perpendicular to the planes. As illustrated in Figure 4(a), it is probable that the signs of the horizontal and vertical Hall voltages will differ for these orders. As an example, the N'eel vector changes from to when C2 is rotated in the direction. The sign of Dxz is changed by this procedure, but the sign of Dxy remains unchanged. This motion induces a reversal in the direction of Vy, whereas Vz remains constant. This kind of switching is illustrated by a SOT device in Figure 4(b). In the presence of a current Jw, usually on the order of 107-108 A/cm2, the N'eel vector is modified by the antidamping spin-orbit torque (SOT). It is possible to find the inverted N'eel vector by examining the Hall voltages Vy and Vz.

IJTBI
International Journal of Technovation and Business Insights
Volume 01, Issue 02, October -December 2025
ISSN: 3107-7900, P.CODE: 25/1-2/04
DOI: https://doi.org/10.5281/zenodo.22305163

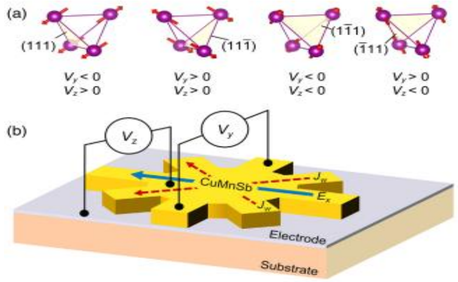

FIG. 4. (a) The signs of the Hall voltages V_y and V_z for different AFM orders of CuMnSb. (b) A spin-orbit torque device where the AFM orders of CuMnSb are switched using the antidampinglike SOT generated by the writing current J_w.

figures 4(a) shows. Assuming a 5 × 106 A=cm2 reading current and a 100-µm sample, we can compute the Hall voltage (Vy) to be between 14 and 90 µV in the dc range .The realm of possible experimental investigations clearly includes this. To everyone's surprise, a high-frequency electric field can cause the Hall current to exhibit a continuous rectified component in addition to a second harmonic component. The nonlinear AHE signal can be isolated from the first harmonic electric field noise in this way. The ability to monitor nonlinear AHE induced by high frequency fields, including picosecond bursts, is made possible by this feature, allowing noncontact technologies to be utilized. Excellent news for efficient ultrafast detection [40,65,66]. A wide variety of AFM materials should contain the nonlinear AHE, and the N'eel vector can be regulated by the antidamping SOT. The AFM metals PdMnTe [67] and Ca3Ru2O7 [68–70] appear like promising candidates to contain a substantial nonlinear AHE in addition to CuMnSb as the heavy metals securely link spin and orbit. We come to the conclusion that the majority of compensated antiferromagnets contain the nonlinear AHE, which hinders SOT and aids in controlling the N'eel vector's electric field. We have proven, using CuMnSb as an example, that it is an antiferromagnet with a big Berry curve dipole, leading to a huge nonlinear AHE. The Berry curvature dipole and the N'eel vector direction have a strong connection. Since it gives a unique technique to verifying the AFM order, this is advantageous for AFM spintronics. Thus, we expect that our theory's predictions will inspire additional research into the nonlinear AHE in antiferromagnets. Speaking with Bo Li and Ruichun Xiao was a treat, and they were tremendously helpful during the writing process. The DMREF program (Grant No. DMR-1629270) and the Nebraska MRSEC program (Grant No. DMR-1420645) of the National Science Foundation (NSF) provided partial funding for this work. This work was made possible by financing from the National Science Foundation of China (NSFC Grant Nos. 11504018 and 11774021). The investigation was done at the University of Nebraska Holland Computing Center.

2. CONCLUSION

The discovery and exploration of the nonlinear anomalous Hall effect (AHE) for Neel vector detection represent a significant milestone in the realm of materials science and spintronics. This unique phenomenon holds immense promise for advancing spintronic devices, particularly in detecting and manipulating the Neel vector in magnetic materials with unprecedented precision and efficiency. The potential applications span across fields such as data storage, spin-based electronics, and quantum computing, opening new avenues for technological innovation.

However, despite the groundbreaking potential, further research and development are imperative to comprehensively understand and harness the nonlinear AHE for practical device implementations. Challenges in optimizing materials, refining detection techniques, and ensuring stability and scalability of devices need to be addressed to realize the full potential of this phenomenon.

Continued interdisciplinary collaboration between physicists, material scientists, and engineers will be instrumental in overcoming these challenges and translating theoretical insights into tangible technological advancements. With sustained efforts and investment in research, the nonlinear anomalous Hall effect for Neel vector detection holds the promise of revolutionizing spintronics and shaping the future of computing and information technology.

REFERENCE

1. T. Jungwirth, X. Marti, P. Wadley, and J. Wunderlich, Antiferromagnetic spintronics, Nat. Nanotechnol. 11, 231 (2016).
2. T. Jungwirth, J. Sinova, A. Manchon, X. Marti, J. Wunderlich, and C. Felser, The multiple directions of antiferromagnetic spintronics, Nat. Phys. 14, 200 (2018).
3. J. Železný, P. Wadley, K. Olejník, A. Hoffmann, and H. Ohno, Spin transport and spin torque in antiferromagnetic devices, Nat. Phys. 14, 220 (2018).
4. L. Šmejkal, Y. Mokrousov, B. Yan, and A. H. MacDonald, Topological antiferromagnetic spintronics, Nat. Phys. 14, 242 (2018).
5. J. Železný, H. Gao, K. Výborný, J. Zemen, J. Mašek, A. Manchon, J. Wunderlich, J. Sinova, and T. Jungwirth, Relativistic N´eel-Order Fields Induced by Electrical Current in Antiferromagnets, Phys. Rev. Lett. 113, 157201 (2014).
6. J. Železný, H. Gao, A. Manchon, F. Freimuth, Y. Mokrousov, J. Zemen, J. Mašek, J. Sinova, and T. Jungwirth, Spin-orbit torques in locally and globally noncentrosymmetric crystals: Anti-ferromagnets and ferromagnets, Phys. Rev. B 95, 014403 (2017).
7. Manchon, J. Zelezný, I. M. Miron, T. Jungwirth, J. Sinova, A. Thiaville, K. Garello, and P. Gambardella, Current-induced spin-orbit torques in ferromagnetic and antiferromagnetic systems, Rev. Mod. Phys. 91, 035004 (2019). [10] P. Wadley et al., Electrical switching of an antiferromagnet, Science 351, 587 (2016).
8. S. Y. Bodnar, L. Šmejkal, I. Turek, T. Jungwirth, O. Gomonay, J. Sinova, A. A. Sapozhnik, H.-J. Elmers, M. Kläui, and M. Jourdan, Writing and reading antiferromag netic Mn2Au by N´eel spin-orbit torques and large aniso tropic magnetoresistance, Nat. Commun. 9, 348 (2018).
9. K. K. Gajula, "Quantum-Enhanced Cryptographic Protocols for Ultra-Secure Data Transmission in Next-Generation Networks," Journal of Dalian University of Technology, vol. 31, no. 12, 2024.
10. K. K. Gajula, "Advancing Post-Quantum Cryptography: Novel Algorithmic Models and Security Implementations," Goya Journal, vol. 18, no. 12, pp. 594–605, 2025.